Kilometer range filamentation

Magali Durand, Aurélien Houard, Bernard Prade, André Mysyrowicz, Anne Durécu, Bernard Moreau, Didier Fleury, Olivier Vasseur, Hartmut Borchert, Karsten Diener, et al.

Kilometer range filamentation

Magali Durand,[1,2] Aurélien Houard,[1] Bernard Prade,[1] André Mysyrowicz,[1] Anne Durécu,[2] Bernard Moreau,[2] Didier Fleury,[2] Olivier Vasseur,[2] Hartmut Borchert,[3] Karsten Diener,[3] Rudiger Schmitt,[3] Francis Théberge,[4] Marc Chateauneuf,[4,*] Jean-François Daigle,[4] and Jacques Dubois[4]

[1] Laboratoire d'Optique Appliquée, ENSTA-ParisTech, Ecole Polytechnique, CNRS, 91762, Palaiseau, France
[2] Onera - the French Aerospace Lab, F-91761 Palaiseau, France
[3] Institut franco-allemand de recherches de Saint-Louis, 68300 Saint-Louis, France
[4] Defence Research and Development Canada (DRDC) Valcartier, 2459 de la Bravoure Road, Québec G3J 1X5, Canada
[*] Marc.Chateauneuf@drdc-rddc.gc.ca

Abstract: We demonstrate for the first time the possibility to generate long plasma channels up to a distance of 1 km, using the terawatt femtosecond T&T laser facility. The plasma density was optimized by adjusting the chirp, the focusing and beam diameter. The interaction of filaments with transparent and opaque targets was studied.

OCIS codes: (190.5940) Self-action effects; (140.7090) Ultrafast lasers; (320.2250) Ultrafast optics: Femtosecond phenomena.

References and links

1. A. Couairon and A. Mysyrowicz, "Femtosecond filamentation in transparent media," Phys. Rep. **441**, 47-189 (2007).
2. S. L. Chin, S. A. Hosseini, W. Liu, Q. Luo, F. Théberge, N. Aközbek, A. Becker, V. P. Kandidov, O. G. Kosareva, and H. Schroeder, "The propagation of powerful femtosecond laser pulses in optical media: physics, applications, and new challenges," Can. J. Phys. **83**, 863-905 (2005).
3. J. Kasparian and J.-P. Wolf, "Physics and Applications of atmospheric nonlinear optics and filamentation," Opt. Express **16**, 466-493 (2008).
4. G. Méchain, A. Couairon, Y.-B. André, C. D'Amico, M. Franco, B. Prade, S. Tzortzakis, A. Mysyrowicz, and R. Sauerbrey, "Long range self-channeling of Infrared laser pulses in air: a new propagation regime without ionization,"Appl. Phys. B **79**, 379-382 (2004).
5. Y. Chen, F. Théberge, O. Kosareva, N. Panov, V. P. Kandidov, and S. L. Chin, "Evolution and termination of a femtosecond laser filament in air," Opt. Lett. **32**, 3477-3479 (2007).
6. F. Théberge, M. Châteauneuf, V. Ross, P. Mathieu, and J. Dubois, "Ultrabroadband conical emission generated from the ultraviolet up to the far-infrared during the optical filamentation in air," Opt. Lett. **33**, 2515-2517 (2008).
7. J. Kasparian, M. Rodriguez, G. Méjean, J. Yu, E. Salmon, H. Wille, R. Bourayou, S. Frey, Y.-B. André, A. Mysyrowicz, R. Sauerbrey, J.-P. Wolf, and L. Wöste, "White-light filaments for atmospheric analysis," Science **301**, 61-64 (2003).
8. D. Comtois, C. Y. Chien, A. Desparois, F. Génin, G. Jarry, T. W. Johnston, J.-C. Kieffer, B. La Fontaine, F. Martin, R. Mawassi, H. Pépin, F. A. M. Rizk, F. Vidal, P. Couture, H. P. Mercure, C. Potvin, A. Bondiou-Clergerie, and I. Gallimberti, "Triggering and guiding leader discharges using a plasma channel created by an ultrashort laser pulse," Appl. Phys. Lett. **76**, 819-821 (2000).
9. S. Tzortzakis, B. Prade, M. Franco, A. Mysyrowicz, S. Huller, and P. Mora, "Femtosecond laser-guided electric discharge in air," Phys. Rev. E **64**, 057401 (2001).
10. G. Méchain, C. D'Amico, Y.-B. André, S. Tzortzakis, M. Franco, B. Prade, A. Mysyrowicz, A. Couairon, E. Salmon, and R. Sauerbrey, "Range of plasma filaments created in air by a multi-terawatt femtosecond laser," Opt. Commun. **247**, 171-180 (2007).
11. R. Salamé, N. Lascoux, E. Salmon, R. Ackermann, J. Kasparian, and J.-P. Wolf, "Propagation of laser filaments through an extended turbulent region," Appl. Phys. Lett. **91**, 171106 (2007).
12. A. Houard, M. Franco, B. Prade, A. Durécu, L. Lombard, P. Bourdon, O. Vasseur, B. Fleury, C. Robert, V. Michau, A. Couairon, and A. Mysyrowicz, "Study of the influence of air turbulence on femtosecond filamentation," Phys. Rev. A **78**, 033804 (2008).
13. Y. R. Shen, "Self-Focusing: Experimental," Prog. Quant. Electr. **4**, 1-34 (1975).
14. V. I. Talanov, "Focusing of light in cubic media," JETP **11**, 199-201 (1970).

15. Q. Luo, S. A. Hosseini, W. Liu, J.-F. Gravel, O. G. Kosareva, N. A. Panov, N. Akozbek, V. P. Kandidov, G. Roy, and S. L. Chin, "Effect of beam diameter on the propagation of intense femtosecond laser pulses**,** " Appl. Phys. B **80**, 35-38 (2005).
16. S. A. Hosseini, Q. Luo, B. Ferland, W. Liu, S. L. Chin, O. G. Kosareva, N. A. Panov, N. N. Aközbek, and V. P. Kandidov, "Competition of multiple filaments during the propagation of intense femtosecond laser pulses," Phys. Rev. A **70**, 033802 (2004).
17. S. Tzortzakis, G. Méchain, G. Patalano, Y.-B. André, B. Prade, M. Franco, A. Mysyrowicz, J.-M. Munier, M. Gheudin, G. Beaudin, and P. Encrenaz, "Coherent sub-THz radiation from femtosecond infrared filaments in air," Opt. Lett. **27**, 1944-1946 (2002).
18. W. Liu and S. L. Chin, "Direct measurement of the critical power of femtosecond Ti:sapphire laser pulse in air," Opt. Express **13**, 5750-5755 (2005).
19. J.-F. Ripoche, G. Grillon, B. Prade, M. Franco, E. Nibbering, R. Lange, and A. Mysyrowicz, "Determination of the time dependence of n_2 in air," Opt. Commun. **135**, 310-314 (1997).
20. A. Brodeur and S. L. Chin, "Ultrafast white-light continuum generation and self-focusing in transparent condensed media," J. Opt. Soc. Am. B **16**, 637-650 (1999).
21. M. Weidman, K. Lim, M. Ramme, M. Durand, M. Baudelet, and M. Richardson, "Stand-off filament-induced ablation of gallium arsenide," Appl. Phys. Lett. **101**, 034101 (2012).

1. Introduction

The long range propagation of laser beams in the atmosphere and their ability to produce intense illumination on distant target has been intensively studied since the discovery of laser. Recently, the observation with femtosecond lasers of a spectacular phenomenon called filamentation has brought new perspectives in this research area [1-3]. During the propagation of a femtosecond pulse in air, provided the initial peak power exceeds a threshold, a dynamic competition between diffraction and nonlinear optical effects such as Kerr effect and plasma defocusing gives rise to thin and long light strings inside which the intensity is clamped to a value above 10^{13} W.cm^{-2}. This filamentation regime characterized by the formation of a weakly ionized plasma channel in the wake of the pulse is followed by a second propagation stage of weaker intensity in which diffraction is only balanced by the Kerr effect [4, 5]. Numerous potential applications have been proposed for filamentation such as the generation of white-light supercontinuum [6], and its application to teledetection of pollutants [7] or the remote guiding of electric discharges [8, 9].

The longest evidence of filamentation and plasma formation has been observed up to 400 m by Méchain *et al.* by propagating horizontally a collimated 4 TW laser beam [10]. For the long distance propagation of such beam, atmospheric turbulence can have a significant effect on the formation of filaments. Recent studies have shown that, once formed, filaments are not very sensitive to turbulence, whereas turbulence undergone before the collapse of the beam by Kerr self-focusing can prevent the apparition of filaments [11, 12].

In this manuscript we will present the details of the experimental setup followed by a characterization of the nonlinear propagation of the TW beam over distances ranging from 150 to 1500 meters. This allowed us to determine the optimal beam parameters to maximize the plasma density at different distances from the laser. The results of the interaction of the long range filaments with different optical windows are then described.

2. Description of the experimental setup

The laser facility used for these experiments was the portable Terawatt & Terahertz (T&T) laboratory from the Defence Research and Development Canada (DRDC) Valcartier. This 5 TW Titanium-doped Sapphire laser system is embedded in a sea container. The compact laser system sits on a 1.25 m by 2.5 m table in a class 100,000 clean room occupying about half of the container. The remaining part being used as a control room and for data acquisition. A schematic of the interior of the T&T laboratory is shown in Fig. 1(a). The control room is filled with the air conditioning unit, the power supplies and chillers for the laser systems as well as the control rack. The laser operator is able to fully control the laser either from the

clean room, the control room or from the exterior of the container via an Ethernet link. The control room also acts as an airlock for the clean room.

The laser pulse energy of the system can reach 200 mJ with pulse duration adjustable from 40 fs up to 15 ps. The pulse repetition rate is 10 Hz, the central laser wavelength is 805 nm and the laser beam diameter at the compressor output is 2.5 cm at full width at half maximum (FWHM).

An all-reflective telescope, composed of a convergent off-axis parabolic mirror with a metallic coating and a divergent dielectric spherical convex mirror mounted on a translation stage, was installed outside the container. The parabolic mirror has a diameter of 15 cm and a focal length of 150 cm. The focal length of the convex mirror is -50 cm which implies a magnification of 3 for a collimated input and output beams. By moving the translation stage it was possible to vary the focusing of the laser beam along its propagating path and therefore, the position of the generated filament. The focal length of the telescope is referred as the geometrical focal length.

These experiments were done at a 2.5 km long firing range located at DRDC Valcartier [see Fig. 1(b)]. The T&T laboratory was installed at one end of the firing range and the laser beam propagated at few meters above the ground. The first 1.5 km of the firing range was flat while the last section was at the base of a mountain.

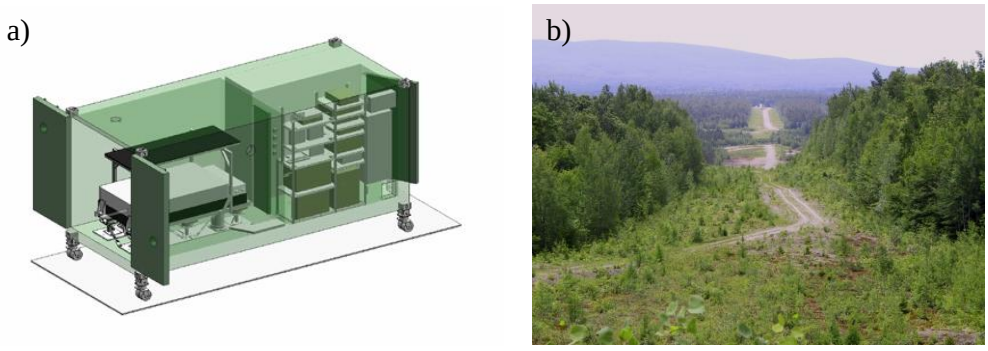

Fig. 1. (a) Schematic of the interior of the T&T container. The clean room with the laser system is shown on the left-hand side and the control room is at the right-hand side of this schema. (b) Picture of the 2.5 km long firing range at DRDC Valcartier, where the tests were conducted.

The propagation of high power laser beam into the atmosphere is characterized by numerous linear and nonlinear optical effects that modify the laser beam energy distribution at long distance. Nonlinear optical effect like the Kerr self-focusing or linear optical effect such as the atmospheric turbulence can strongly decrease the achievable laser intensity at long distance. Reaching high laser intensity at long range in the atmosphere with a compact optical device remains a challenge. Solutions for delivering the high laser intensity at distance involve the use of optical components that pre-compensate for the perturbations induced by the linear propagation effects and modify the laser beam parameters in order to minimize the undesired nonlinear intensity-dependent optical effects.

Because of the self-focusing in air, it is important to adjust the initial intensity of the laser pulses with both the optical compressor and a beam expander in order to optimize the generation of filaments at longer distances. The main concept behind the idea of using a beam expander to induce filaments at long distance is based on the self-focusing property of powerful and ultrashort laser pulses. The self-focusing distance (z_f) of a laser pulse, which is approximately the starting point of the filament, is given by [13]:

$$z_f = \frac{0.367ka^2}{\left\{\left[\left(\frac{P}{P_{cr}}\right)^{1/2} - 0.852\right]^2 - 0.0219\right\}^{1/2}}, \quad (1)$$

where P_{cr} is the critical power for self-focusing, k is the wavevector of the laser pulse, a is the beam radius defined at 1/e level of the intensity and P is the initial peak power of the laser pulse. Thus, a laser beam having a larger radius (parameter a is larger) would tend to self-focus at longer distance. Moreover, decreasing the ratio P/P_{cr} (by adjusting the energy per pulse, the pulse duration and/or the laser chirp) would also increase the self-focusing distance (z_f).

In the presence of the external focusing from the sending telescope, the new self-focusing distance z_f' becomes [14]:

$$z_f' = \frac{z_f f_{eff}}{z_f + f_{eff}}, \quad (2)$$

in which f_{eff} denotes the effective focal length of the telescope. Thus, if we adjust the radius of the beam (a) and its peak power (P) in such a way $z_f >> f_{eff}$, then $z_f' \cong f_{eff}$ and the filament is generated around the geometrical focus of the telescope.

Working with intense and ultrashort laser pulses is different than with a conventional laser beam. The spectrum of the pulse is large (tens of nm) which is subject to chromatic aberrations. More importantly, undesired non-linear effects are much more important in glass than in air and the self-focusing in refractive optics tends to generate "hot spots" in the laser beam profile, which decreases the effective radius of the laser beam and makes the laser beam to self-focus at shorter distances [15, 16]. That justifies the choice of using an off-axis all reflective telescope instead of an on-axis telescope composed of transparent lenses.

3. Characterization of the propagation

3.1 Optimization of the beam parameters

Our goal was to demonstrate the possibility to achieve kilometer range femtosecond filamentation and to study the interaction of such long range filaments on different optical windows. We studied the long range filamentation at the following distances of observation D_i: D_1 = 150 m, D_2 = 300 m, D_3 = 500 m, D_4 = 1 km and finally D_5 = 1.5 km. For each distance D_i the plasma density yields locally was optimized by adjusting the chirp, the magnification and the focal length of the telescope. The plasma density was monitored using an electronic detector sensitive to radiation around 10 GHz placed on the side of the filament. This signal radiated by the plasma permits to evaluate the local plasma density and to determine the best beam parameters to produce a maximum of filaments at this position [17]. From these measurements we determined that the optimal focusing corresponds to a geometrical focus a few meters after the observation position, while the optimal chirped pulse durations were respectively 1.2 ps, 3.68 ps and 2.97 ps for 150 m, 300 m and 1 km. When comparing the value of negative chirp impressed on the pulse and the value of air dispersion, one can see that in every cases the dispersion of air was negligible compared to the chirp of the pulse. The purpose of chirping the pulse was then not to pre-compensate the dispersion of air but to postpone the filament formation by decreasing the initial peak power.

3.2 Length and number of filaments as a function of the distance

For each distances D_i, the length and the number of plasma filaments were measured by impact on photographic paper at different positions around the geometrical focus. Results are

presented in Fig. 2 where the black dots symbolize the distance at which an impact was made revealing the presence of a plasma channel. The grey lines symbolize the presence of light channels, which are millimeter size lower intensity channel emerging from the 100 μm plasma filaments [4, 5]. The inset in Fig. 2 shows an example of traces made by a filament and by a light channel on the photographic paper. The light channels allow the energy of the pulse to continue to travel with a minimal diffraction over several hundred of meters but they are not intense enough to ionize air. At 1.5 km, plasma channels were not achieved, at this distance only light channel were observed. Those experiments confirm the result of Méchain *et al.*, who showed that plasma channels evolve into light channels in the case of long distance femtosecond filamentation.

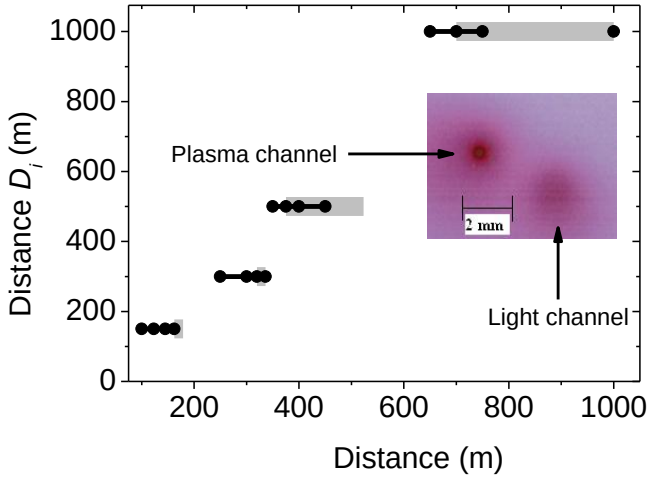

Fig. 2. Measurement of position of the plasma channels (black dot) and the position of the light channels (grey large line) for different distances D_i. Inset: impacts on a photographic paper showing a plasma channel and a light channel at 700 m for optimized parameters at 1 km.

For each value of D_i the length over which ionization occurs was estimated. As shown in Fig. 3 this length increases linearly with the distance of optimization D_i and reaches 350 m when the beam is optimized at 1 km. At the same time the averaged number of filaments across the laser beam profile decreases from 17 to ~ 3 beyond 300 m and keeps roughly the same value until 1 km. We note that this number is in direct correlation with the ratio P/P_{cr} where

P_{cr} = 5 GW is the critical power for self-focusing in air at 800 nm for pulse duration longer than 200 fs [18]. Indeed, P/P_{cr} was equal to 40 at 150 m and dropped to ~13 for larger distances. This correlation is in good agreement with theoretical predictions [1].

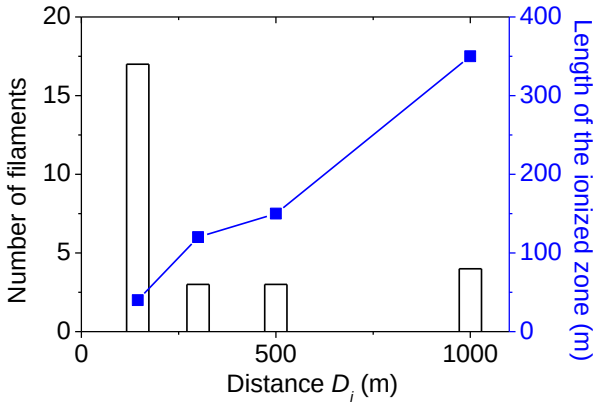

Fig. 3. Measurement of the length over which ionization occurs (square) and average number (bars) of filaments across the laser profile as a function of the value of Di.

3.3 Evolution of the laser spectrum at 1 km as a function of the chirp

The spectrum of the laser recorded after propagation shows strong modifications due to nonlinear interactions depending on the intensity of the initial pulse. The inset of Fig. 4 shows two typical results obtained after 1 km propagation corresponding to an initial pulse duration of 0.84 ps (red curve) and 6 ps (black curve) respectively. The comparison of the two curves shows that the pulse corresponding to the shorter duration, which is also the most intense, undergoes a global redshift. The red points in Fig. 4 show the variation of the mean wavelength as a function of the initial pulse duration, when the pulse duration was varied by imposing a negative chirp.

We attribute the Stokes shift of the propagated spectrum to the retarded Kerr effect in air [19] and develop a very simplified model in order to explain more quantitatively our measurements. By taking into account only phase effects and neglecting diffraction and ionization, the evolution of the electric field E in the semi-wave approximation reads: $dE/dz = i\,k\,n(t)\,E$ where k is the wavenumber and $n(t)$ represents an intensity dependent index of refraction. By taking the Fourier transform of the electric field E, we obtain the evolution equation of the spectrum F:

$$\frac{dF}{dz} = ik\int_{-\infty}^{+\infty} n(t)E\,\mathrm{e}^{i2\pi\nu t}dt. \tag{3}$$

By multiplying each member of Eq. (3) and adding the complex conjugate, we obtain the propagation equation of the modulus of the spectrum:

$$\frac{d|F|^2}{dz} = ik\int_{-\infty}^{+\infty} n(t)EF*\mathrm{e}^{i2\pi\nu t}dt + \mathrm{C.C.} \tag{4}$$

We characterize the redshift by computing the mean frequency <ν> of the spectrum defined by

$$\langle\nu\rangle = \frac{\int_{-\infty}^{+\infty}\nu|F(\nu)|^2\,d\nu}{\int_{-\infty}^{+\infty}|F(\nu)|^2\,d\nu}. \tag{5}$$

$$\frac{d\langle\nu\rangle}{dz} = ik\int_{-\infty}^{+\infty}\nu d\nu\int_{-\infty}^{+\infty} n(t)EF*\mathrm{e}^{i2\pi\nu t}\,dt \Big/ \int_{-\infty}^{+\infty} I(t)dt + \mathrm{C.C.} \tag{6}$$

By using the property of the inverse Fourier Transform, we obtain after integration over ν

$$\frac{d\langle\nu\rangle}{dz} = \frac{k}{2\pi}\int_{-\infty}^{+\infty} n(t)E\frac{dE^*}{dt}dt \Big/ \int_{-\infty}^{+\infty} I(t)dt + \text{C.C.} \tag{7}$$

and finally $\frac{d\langle\omega\rangle}{dz} = k\int_{-\infty}^{+\infty} n(t)\frac{dI}{dt}dt \Big/ \int_{-\infty}^{+\infty} I(t)dt$, where $\omega = 2\pi\nu$ is the circular frequency. Let us now specify *n(t)* and *I(t)*. The retarded Kerr effect can be modeled by the expression:

$$n(t) = \frac{n_2}{\tau}\int_0^{+\infty} e^{-u/\tau} I(t-u)du, \tag{8}$$

where n_2 is the instantaneous Kerr effect coefficient and τ is the delay. Recall that the variations of the pulse duration are obtained by moving the distance between the compressor gratings. Under this condition the intensity depends on pulse duration in order to keep the energy constant. We model the intensity *I(t)* by an expression of the form $I(t) = \frac{\Delta t_0}{\Delta t} I_0 \exp(-t/\Delta t)^2$ which represents the intensity envelope of a chirped pulse of duration Δt and energy $\Delta t_0 I_0 \sqrt{\pi}$ independent of the duration. Here Δt_0 corresponds to the minimum pulse duration obtained for the compressed pulse.

By using the expressions of *n(t)* and *I(t)* the evolution of the mean frequency is given by the following integral :

$$\frac{d\langle\omega\rangle}{dz} = -\frac{2kn_2 I_0 \Delta t_0}{\tau(\Delta t)^4\sqrt{\pi}}\int_{-\infty}^{+\infty}\int_0^{+\infty} t\, e^{-t^2/\Delta t^2}\, e^{-u/\tau}\, e^{-(t-u)^2/\Delta t^2}\, dt\,du. \tag{9}$$

The integration gives:

$$\frac{d\langle\omega\rangle}{dz} = -\frac{kn_2 I_0 \Delta t_0}{2\tau\sqrt{\pi}}\left\{\frac{\sqrt{2\pi}}{\Delta t} + \frac{\pi}{\tau} e^{\Delta t^2/2\tau^2}\left[erf\left(\frac{\Delta t\sqrt{2}}{2\tau}\right)\right] - 1\right\}. \tag{10}$$

In practice, for the values of τ and Δt considered here the second term is negligible so that $d\langle\omega\rangle/dz = -kn_2 I_0 \Delta t_0/\Delta t\tau\sqrt{2}$. Finally the redshift after a length of propagation z is given by:

$$\frac{\Delta\langle\lambda\rangle}{\lambda_0} = -\frac{\Delta\langle\omega\rangle}{\omega_0} = \frac{kn_2 I_0}{\tau\sqrt{2}\omega_0}\frac{\Delta t_0}{\Delta t} z, \tag{11}$$

showing that the redshift is inversely proportional to the pulse duration Δt. Figure 4 shows (black curve) the centroid wavelength redshift computed according to Eq. (11). This model although very simplified is in good agreement with the measurements (red dots).

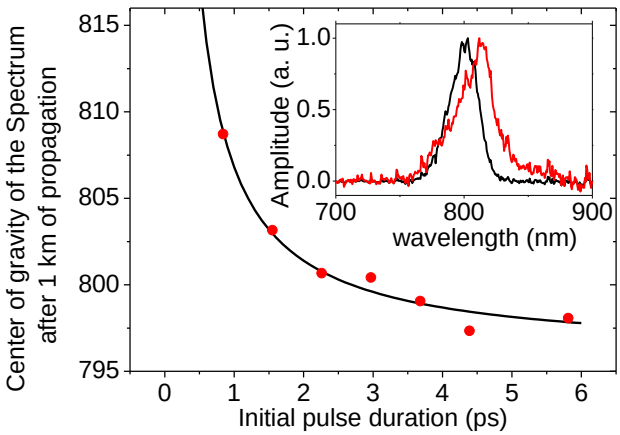

Fig. 4. Red shift of the spectrum after 1 km of propagation in air as a function of the initial pulse duration. Measurements (red point) and calculation (continuous black curve) based on Eq. (11). Insert: spectrum for 6 ps (black curve) and spectrum for 0.84 ps (red curve).

4. Interaction between long range filaments and solid materials

4.1 White-light generation at long distance up to 1.5 km in transparent materials for visible spectrum

We studied at different distances the ability of the filaments to generate conical white light in transparent windows made of Silica, CaF_2, BK7 and Sapphire, materials which are well suited for supercontinuum generation [19]. For the optimized distances D_i between 150 m and 1 km, the presence of high intensity filaments gave rise to significant white light generation. The continuum generated by the filaments in the material was observed on a diffusing screen, and a collecting lens was used to image the whole cone of white light into the fiber of the spectrometer. Measured spectra at 500 m are presented in Fig. 5, where each curve is an average over 10 shots. The black curve is the spectrum of the beam in absence of windows. One can see that the contribution of white light emitted by the solids is not negligible over the white light emitted by the filamentation in air. On average the continuum created in the transparent materials was detected from 400 nm to 1.1 μm. As for the number of filaments presented in Fig. 3, we observe a drop in the efficiency of supercontinuum generation in solids after 150 m and then a stable production until 1 km. Only light channels were obtained at the optimized distance of 1.5 km. Those light channels were also powerful enough to induce filamentation in transparent windows and to produce white light emission.

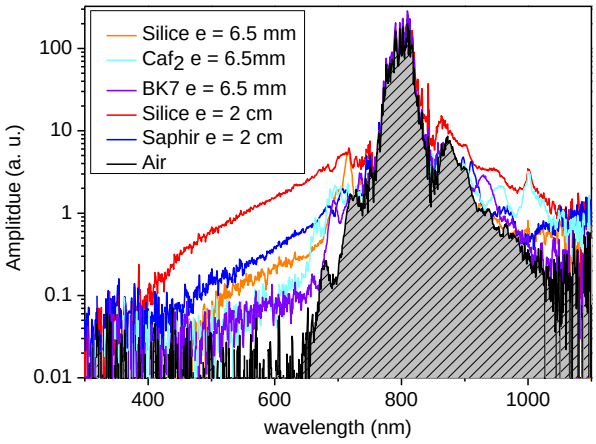

Fig. 5. Generated spectrum in different transparent materials after a propagation of 500 m. The black curve shows the spectrum of the laser pulse before the sample.

4.2 Long range filament effects on IR materials

Different impact tests were performed during this study by changing the distance between the laser source and Germanium samples, the chirp, and the telescope magnification. The measurements have been performed under different weather conditions. The distance between the laser source and the sample was changed from 30 m up to 1300 m. The damage effect on the sample of a single shot and several thousand laser pulses was studied. The weather conditions were measured to investigate the influence of these effects on the filamentation and damaging behaviour. Chirp values varying between 1 ps and 4.3 ps were used to reach a maximum of energy in the filaments for different distances and different weather conditions. Figure 6 presents the damage on Ge samples.

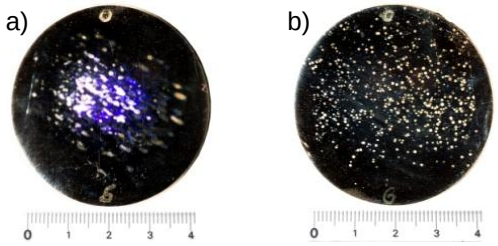

Fig. 6. Damage impacts on Ge at different distances (left: 500 m, right: 1000 m).

The damage caused to Ge remains on the surface. Even with one pulse, the Ge window could be damaged at some points on the surface. The high intensity in the filaments caused this punctual damage behavior [20]. Displacement of the filaments inside each laser pulse profile caused damages on different position of the Ge irradiated surface. Thus for a series of 600 pulses the whole irradiated surface was damaged. The damage decreases with longer distances and depends also on the weather conditions. Concerning weather conditions we can resume that turbulences and fog reduce the damage impact on the IR-windows, but normal rain does not reduce the damage behavior.

5. Conclusion

In conclusion, by optimizing the parameters of beam diameter, focalization and chirp we managed to sustain plasma channels formation over 350 m at a target distance of 1 km. It was

demonstrated that the effect of chirping the pulse is postponing the filament formation by decreasing the initial peak power and not pre-compensating the dispersion of air. The supercontiuum generated in transparent solids is detected from 400 nm to beyond 1.1 μm with different efficiency depending on the material. Above 1 km the filaments transform into intense bright light channels. At 1.5 km, such light channels were observed and were able to induce filamentation in transparent windows with white light supercontiuum generation.

We have shown also that the high intensity filament core is responsible for the damages measured on Germanium samples. Germanium samples could be damaged by means of filaments in the km range. The damage thresholds for Ge samples are much lower with femtosecond laser pulses than for longer laser pulses. Tests have shown that damage effects are possible under free-field propagation conditions. Concerning weather conditions we can resume that turbulences and fog reduce the damage impact on the IR-windows, but normal rain does not reduce the damage behavior.

Acknowledgments

We acknowledge the support from a DRDC Applied Research Program and a DRDC Technology Investment Fund and from Délégation Générale pour l'Armement DGA through grant REI 2009 34 0025. We thank also the technical support from Michèle Cardinal, Marcellin Jean and Alain Fernet from DRDC and the participation of Bruno Desruelle from DGA.